MDPI

Article

Effect of Deposition Parameters on Morphological and Compositional Characteristics of Electrodeposited CuFeO$_2$ Film

Min-Kyu Son

Nano Convergence Materials Center, Emerging Materials R&D Division, Korea Institute of Ceramic Engineering & Technology (KICET), Jinju 52851, Republic of Korea; minkyu.son@kicet.re.kr; Tel.: +82-55-792-2683

Abstract: Deposition parameters determine the characteristics of semiconductor films in electrodeposition. Thus, it is essential to understand the effect of deposition parameters on the electrodeposited film for fabricating suitable semiconductor film fitting for various applications. In this work, the morphological and compositional properties of electrodeposited delafossite CuFeO$_2$ film, according to the deposition parameters, were studied. The CuFeO$_2$ film was fabricated by the galvanostatic electrodeposition and post-annealing process under inert gas flow. The type of solvent, electrolyte condition, applied current density and deposition time were controlled as the variable deposition parameters. As a result, the typical CuFeO$_2$ film, without any impurities, was electrodeposited in the electrolyte-based DMSO solvent. Interestingly, the concentration of potassium perchlorate as a complexing agent caused morphological change in electrodeposited CuFeO$_2$ film, as well as compositional transition. On the other hand, the applied current density and deposition time only influenced the morphology of electrodeposited CuFeO$_2$ film. These observations would provide specific guidelines for the fabrication of electrodeposited CuFeO$_2$ film with suitable composition and morphology for various applications.

1. Introduction

Delafossite-structured CuFeO$_2$ has attracted much interest in various research fields due to its inherent characteristics, as shown in Table 1. It has been widely used as a transparent conductive film owing to its high p-type conductivity [1–3]. It also shows a relatively high Seebeck coefficient, which is beneficial in temperature sensor applications [4,5]. In addition, it exhibits a unique magnetic behavior, inducing phase transition at low temperature by antiferromagnetic interactions between Fe^{3+} ions in CuFeO$_2$. Hence, it can be utilized in multifunctional magnetoelectric devices [6,7]. Contrary to other wide band gap delafossite materials, its band gap is visibly light-responsive (1.1~1.6 eV) [8,9]. Therefore, in recent years, it has been extensively investigated in solar energy conversion devices, such as solar cells [10,11], photoelectrochemical photocathodes for water splitting [9,12–16] and photocatalysts [17–19].

Table 1. General characteristics of delafossite-structured CuFeO$_2$ [1–3,8,9,16].

Characteristics	Values
Conductivity	1.53~2 S cm^{-1}
Carrier mobility	0.2 cm^2 V^{-1} s^{-1}
Hall coefficient	1.84 × 10^6 m^2 C^{-1}
Band gap	1.1~1.6 eV
Absorption coefficient	Up to 10^7 m^{-1}

CuFeO$_2$ thin film has been considered as a one-size-fits-all electrode in these application devices. It has been synthesized via various deposition techniques such as sputtering [2,20–22], pulsed laser deposition [23–25], sol-gel based spin coating [1,26,27], hydrothermal method [19,28], electrodeposition [9,29–31] and spray pyrolysis [3,32,33]. Among these deposition techniques, the electrodeposition is an advantageous method for fabrication of high-quality CuFeO$_2$ thin film. First, it is cost-effective because it does not need expensive vacuum facilities, contrary to sputtering or pulsed laser deposition. The only necessary tools for electrodeposition are an electrolyte bath and a potentiostat to apply the potential or current. Second, it is an energy-saving deposition method because the process temperature is mild (room temperature or below 100 °C), unlike the hydrothermal method or spray pyrolysis. Third, it is easily scalable in a large area bath, facilitating the fabrication of large area CuFeO$_2$ electrodes [34,35].

Read et al. successfully fabricated an electrodeposited CuFeO$_2$ photocathode using a deposition solution based on dimethyl sulfoxide (DMSO) solvent [9]. This deposition solution also includes 1 mM copper (II) nitrate, 3 mM iron (III) perchlorate, and 100 mM potassium perchlorate. Crystalline CuFeO$_2$ film with a thickness of 100~130 nm was fabricated by the potentiostatic mode for 20 min and the sequential annealing process under inert gas atmosphere. Riveros et al. also obtained CuFeO$_2$ thin film from DMSO based deposition solution [36]. They studied the characteristics of electrodeposited CuFeO$_2$ film by controlling the potential and the anion type in the deposition solution. As a result, stoichiometric CuFeO$_2$ film was grown by the electrodeposition with an applied potential of -0.6 V in perchlorate/chloride anions-mixed DMSO solution. Kang et al. fabricated CuFeO$_2$ and CuO composite films by potentiostatic electrodeposition using aqueous solution containing 4 mM copper (II) nitrate, 12 mM iron (III) perchlorate and 50 mM potassium perchlorate [37]. It was revealed that the morphology of a deposited CuFeO$_2$/CuO film based water solution is quite different when compared with the DMSO solution. The whole electrodeposition process is almost identical in the relevant literature. Nevertheless, the detailed electrodeposition conditions are slightly different. In electrodeposition, deposition parameters such as potential, current density, time and electrolyte composition determine the characteristics of the CuFeO$_2$ film [38]. Therefore, it is important to control these during the electrodeposition process to obtain the desired CuFeO$_2$ film in accordance with the specific application. Furthermore, it is essential to study the effect of deposition parameters on the characteristics of electrodeposited CuFeO$_2$ film.

Thus, in this study, the morphological and compositional characteristics of electrodeposited CuFeO$_2$ film, depending on these conditions, were investigated. Two types of solvent were selected: DMSO and water, which are typical solvents for electrodepositing CuFeO$_2$ film. The concentration of chemical salts in the electrolyte was chosen from representative recipes in previous literature [9,36,37]. The CuFeO$_2$ film was electrodeposited by galvanostatic mode, enabling precise thickness control. The current and deposition time were also controlled because they are significant deposition parameters that determine the property of an electrodeposited film in galvanostatic electrodeposition. Herein, the understanding of the characteristics of the electrodeposited CuFeO$_2$ film, depending on these electrodeposition parameters, would provide guidelines for selecting suitable deposition conditions to fabricate the optimal electrodeposited CuFeO$_2$ electrode fitting for specific applications.

2. Materials and Methods

DMSO (C$_2$H$_6$SO, 99.9%, Sigma Aldrich, St. Louis, MO, USA) and distilled water were used as the solvent to prepare the electrolyte for electrodeposition. To examine the solvent effect, electrolyte containing 1 mM copper (II) nitrate hydrate (Cu(NO$_3$)$_2$·xH$_2$O, 99.999%, Sigma Aldrich, St. Louis, MO, USA), 3 mM iron (III) perchlorate hydrate (Fe(ClO$_4$)$_3$·xH$_2$O, Sigma Aldrich, St. Louis, MO, USA), and 100 mM potassium perchlorate (KClO$_4$, 99%, Sigma Aldrich, St. Louis, MO, USA) was prepared. On the other hand, electrolyte with more concentration of Cu/Fe salts and less concentration of KClO$_4$ was prepared to study

the effect of electrolyte composition on $CuFeO_2$ film. It contained 4 mM $Cu(NO_3)_2 \cdot xH_2O$, 12 mM $Fe(ClO_4)_3 \cdot xH_2O$ and 50 mM potassium perchlorate. The ratio of Cu and Fe was fixed to 1:3 in all electrolytes for electrodeposition.

The $CuFeO_2$ film was electrodeposited on a cleaned fluorine-doped tin oxide (FTO) glass substrate (surface resistivity 7 Ω sq^{-1}, Sigma Aldrich, St. Louis, MO, USA). The cleaning process of FTO glass substrates consisted of ultrasonication for 30 min then O_2 plasma treatment (CUTE, FEMTO Science, Hwaseong, Republic of Korea) for 10 min. The ultrasonication was carried out in the order of acetone, ethanol, and distilled water and each process was carried out for 10 min. The electrodeposition was carried out in the prepared electrolyte via the galvanostatic mode using a standard three electrode system. It was composed of the FTO glass substrate as a working electrode, the Pt wire as a counter electrode and the Ag/AgCl electrode in saturated KCl as a reference electrode. Constant current density was applied by a potentiostat (HSV-100, Hokuto Denko, Tokyo, Japan) during electrodeposition at room temperature for various deposition time periods. Finally, the electrodeposited $CuFeO_2$ film was annealed at 650 °C for 1 h with a ramp ratio of 5 °C min^{-1} under inert N_2 gas flow.

The morphological characteristics of fabricated $CuFeO_2$ films was analyzed by a high-resolution scanning electron microscope (SEM, JSM-7900F, JEOL Ltd., Tokyo, Japan). In the SEM analyses, the accelerating voltage was 5.0 kV, while the working distance was 10.0 mm. The element analysis on the $CuFeO_2$ film surface was conducted by an energy dispersive X-ray (EDX, Oxford Instrument, Abingdon-on-Thames, UK) analyzer attached to the SEM system. The crystallographic analyses were performed using a high-resolution X-ray diffraction system (XRD, SmartLab 9 kW AMK, Rigaku Corporation, Tokyo, Japan) and an Arc cluster ion beam X-ray photoelectron spectroscopy system (XPS, PHI 5000 Versa Probe II, ULVAC, Kanagawa, Japan). The XRD measurement was carried out in the range of 2θ = 20° to 70° with a step width of 0.02° and a scan rate of 2° min^{-1} using a Cu-Kα radiation source. Measured XPS spectra were fitted by the PHI Multipak software.

3. Results and Discussion

Non-aqueous based electrodeposition does not form metal hydroxide during the electrodeposition process, contrary to aqueous based electrodeposition. Thus, it influences the property of electrodeposited thin film. To examine this influence, the $CuFeO_2$ film was electrodeposited using DMSO or distilled water solution with 1 mM $Cu(NO_3)_2 \cdot xH_2O$, 3 mM $Fe(ClO_4)_3 \cdot xH_2O$ and 100 mM potassium perchlorate. Figure 1 shows the XRD patterns of the electrodeposited film in the electrolyte based DMSO and water solvents by applying a current density of −0.2 mA cm^{-2} for 60 min with post-annealing treatment at 650 °C for 1 h under N_2 gas flow. All samples have diffraction peaks related to SnO_2 (JCPDS No. 46-1088) from the FTO glass substrate. The diffraction peaks at 2θ = 31.26° and 35.8°, attributed to (006) and (012) orientations of the crystalline $CuFeO_2$ (JCPDS No. 0175-2146) [39–41], were observed in the electrodeposited film in the DMSO solution. No other diffraction peaks, including those of metallic Cu or Fe, were observed. This means that electrodeposition using a DMSO solvent and post-annealing process produces a well-crystalline $CuFeO_2$ film without any impurities. On the other hand, diffraction peaks at 2θ = 36.4° and 42.3°, corresponding to (111) and (200) orientations of the crystalline Cu_2O (JCPDS No. 05-0667) [42,43], respectively, were observed in the electrodeposited film in the water solution. This indicates that the electrodeposited film in the water solution is the Cu_2O film and not the $CuFeO_2$ film.

The reason for this difference can be found in the mechanism of electrodeposition in different solvents. In general, the electrodeposited $CuFeO_2$ film was formed by co-deposition of Cu_2O and Fe_2O_3 via the following reactions [36]:

$$Fe^{3+}_{(sol)} + e^- \rightarrow Fe^{2+}_{(sol)} \tag{1}$$

$$Cu^{2+}_{(sol)} + e^- \rightarrow Cu^+_{(sol)} \tag{2}$$

$$2 \, Fe^{2+}_{(sol)} + 3/2 \, O_{2(sol)} + 4 \, e^- \rightarrow Fe_2O_{3(s)} \tag{3}$$

$$2 \, Cu^+_{(sol)} + 1/2 \, O_{2(sol)} + 2 \, e^- \rightarrow Cu_2O_{(s)} \tag{4}$$

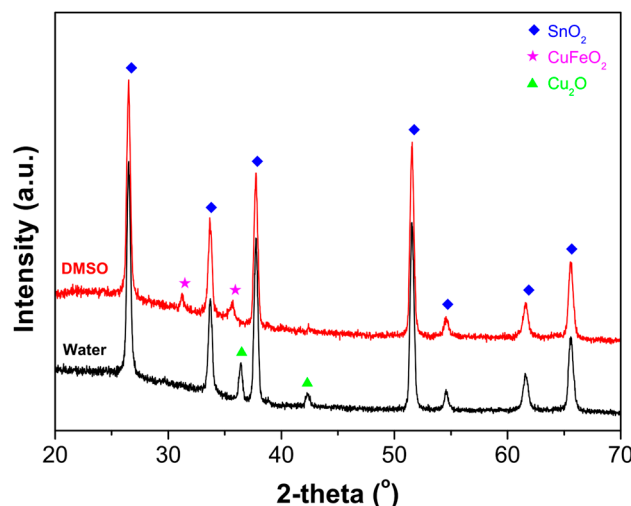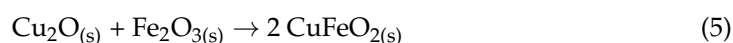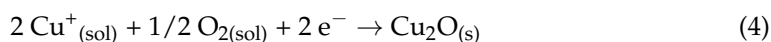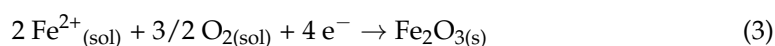$$Cu_2O_{(s)} + Fe_2O_{3(s)} \rightarrow 2 \, CuFeO_{2(s)} \tag{5}$$

Figure 1. XRD patterns of electrodeposited film in electrolyte-based DMSO (red) and water (black) solvents. Electrodeposition was carried out by applying a current density of -0.2 mA cm^{-2} for 60 min and the films were annealed at 650 °C for 1 h under N$_2$ gas flow after electrodeposition.

In these reactions, the formation of Cu$_2$O is more favored than that of Fe$_2$O$_3$ because the former is kinetically preferred to the latter [36]. Hence, the Cu$_2$O film was formed in the electrodeposition using the water solution. Meanwhile, molecules of DMSO ((CH$_3$)$_2$SO) form strong complexes with copper (II) ions in the copper (II) nitrate hydrate [44]. This stabilizes the Cu ions in the electrodeposition bath, accelerating the Fe deposition in the film. Therefore, the CuFeO$_2$ film was formed in the electrodeposition using DMSO solution.

The pristine electrodeposited CuFeO$_2$ film from the DMSO solution was amorphous because no diffraction peaks were detected, except those related to the SnO$_2$ from the FTO substrate (Figure S1). This means that the post-annealing treatment at 650 °C under N$_2$ gas flow is necessary to transform the amorphous CuFeO$_2$ into the crystalline one. In addition, it is clearly shown that the crystalline CuFeO$_2$ film was homogeneously distributed, by element mapping of Cu, Fe and O from the top-view EDX characterization (Figure S2). Moreover, from the EDX characterization, it was demonstrated that the atomic ratio of Cu:Fe is almost 1:1 (9.87:8.88), which also indicates that the electrodeposited CuFeO$_2$ film is stoichiometric. This suggests that the homogeneous and stoichiometric crystalline CuFeO$_2$ film is successfully fabricated by the electrodeposition using a DMSO-based solution and post-annealing process under inert gas flow.

A complexing agent in the deposition electrolyte has been introduced to activate the Fe deposition for the electrodeposited CuFeO$_2$ film. Therefore, it could have affected the characteristic of electrodeposited CuFeO$_2$ film. Potassium perchlorate has been used to provide the chloride anion as a complexing agent in the electrodeposition of CuFeO$_2$ film [9,36,37]. To investigate the effect of the complexing agent on the characteristics of electrodeposited CuFeO$_2$ film, the electrodeposition was carried out using electrolyte with different potassium perchlorate concentrations. Figure 2 exhibits the XRD patterns of electrodeposited CuFeO$_2$ film by applying a current density of -0.2 mA cm^{-2} for 60 min in the DMSO based electrolyte containing 1 mM Cu(NO$_3$)$_2$·xH$_2$O/3 mM Fe(ClO$_4$)$_3$·xH$_2$O/100 mM potassium perchlorate (Solution #1) and 4 mM Cu(NO$_3$)$_2$·xH$_2$O/12 mM Fe(ClO$_4$)$_3$·xH$_2$O/50 mM potassium perchlorate (Solution #2) after the post-annealing treatment at 650 °C under N$_2$ gas flow. The diffraction peaks at $2\theta = 31.26°$ and $35.8°$ are well matched with (006) and (012) orientations of the crystalline CuFeO$_2$ in the electrodeposited film in Solution

#1. On the other hand, in the electrodeposited film in Solution #2, the diffraction peak corresponding to the (006) orientation of $CuFeO_2$ was also observed. However, the diffraction peak related to the (012) orientation of $CuFeO_2$ was slightly shifted to the large angle ($35.8° \rightarrow 36.26°$). It is assumed that the characteristic of $CuFeO_2$ film was affected by the lattice parameter change or defect density [45]. In addition, the diffraction peak ($2\theta = 42.3°$) attributed to the (111) orientation of the crystalline Cu_2O was observed. This indicates that Cu_2O was formed as the impurity when the film was electrodeposited in Solution #2.
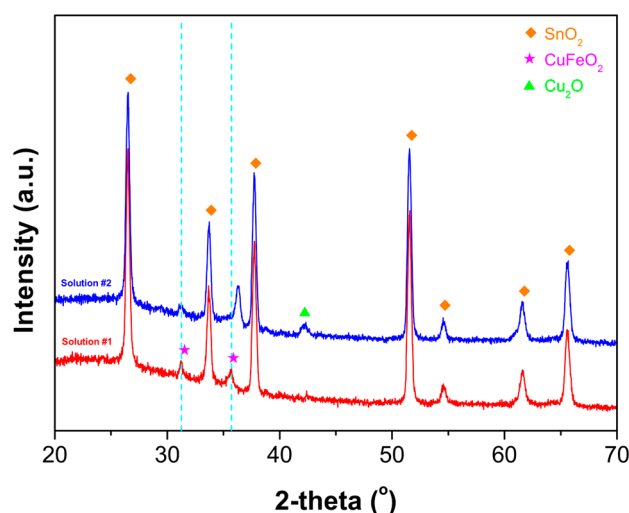

Figure 2. XRD patterns of electrodeposited $CuFeO_2$ film by applying a current density of -0.2 mA cm^{-2} for 60 min in DMSO based electrolytes with different potassium perchlorate concentrations. Solution #1 (red) contained 1 mM $Cu(NO_3)_2 \cdot xH_2O$/3 mM $Fe(ClO_4)_3 \cdot xH_2O$/100 mM potassium perchlorate, while Solution #2 (blue) contained 4 mM $Cu(NO_3)_2 \cdot xH_2O$/12 mM $Fe(ClO_4)_3 \cdot xH_2O$/50 mM potassium perchlorate. Electrodeposited films were annealed at 650 °C for 1 h under N_2 gas flow.

Besides this, the morphologies of two films were totally different. As shown in Figure 3, irregularly shaped particles were covered in the electrodeposited film in Solution #1 (Figure 3a), while spherically shaped particles were deposited in the electrodeposited film in Solution #2 (Figure 3b). The average particle size was approximately 220 nm and some particles were agglomerated in the electrodeposited film in Solution #1. Meanwhile, the average particle size was approximately 315 nm and no particle aggregations were observed in the electrodeposited film in Solution #2. Based on these observations, it was concluded that the electrolyte containing more potassium perchlorate is adequate for making the pure crystalline $CuFeO_2$ film with small particles using the galvanostatic electrodeposition. It is also demonstrated that the concentration of Cu/Fe salts was not a dominant factor determining the characteristic of the electrodeposited $CuFeO_2$ film in the electrolyte condition, with a fixed ratio of Cu:Fe = 1:3.

The applied current density was controlled during the electrodeposition in the DMSO based electrolyte containing 1 mM $Cu(NO_3)_2 \cdot xH_2O$/3 mM $Fe(ClO_4)_3 \cdot xH_2O$/100 mM potassium perchlorate to study the property of the electrodeposited $CuFeO_2$ film according to the current density in the galvanostatic mode. Figure 4a show the XRD patterns of the electrodeposited $CuFeO_2$ film for 30 min by applying different current densities after post-annealing treatment at 650 °C under N_2 gas flow. As illustrated in Figure 4a, all films have diffraction peaks at $2\theta = 31.26°$ and $35.8°$, attributed to the (006) and (012) orientations of the crystalline $CuFeO_2$. Although they are weaker than those in the $CuFeO_2$ electrodeposited for 60 min, due to the short deposition time, it clearly supports that the deposited film was the crystalline $CuFeO_2$ without any impurities. In other words, the current density of galvanostatic electrodeposition did not have any influence on the composition of the electrodeposited film. However, it affected the morphology of the electrodeposited $CuFeO_2$ film, as shown in Figure 4b–d. The irregular shaped $CuFeO_2$ particles were formed on the

substrate, similar to that in Figure 3a, while the aggregation of $CuFeO_2$ particles became large when the applied current density was increased. This was likely to be due to the distinction of deposition speed, depending on the current density. The Cu/Fe ions in the solution were quickly moved to the substrate's surface or pre-deposited $CuFeO_2$ film by the strong electric field when the large current density was applied. Hence, the aggregation became severe around the previously deposited $CuFeO_2$ particles in the electrodeposited film with the large current density.
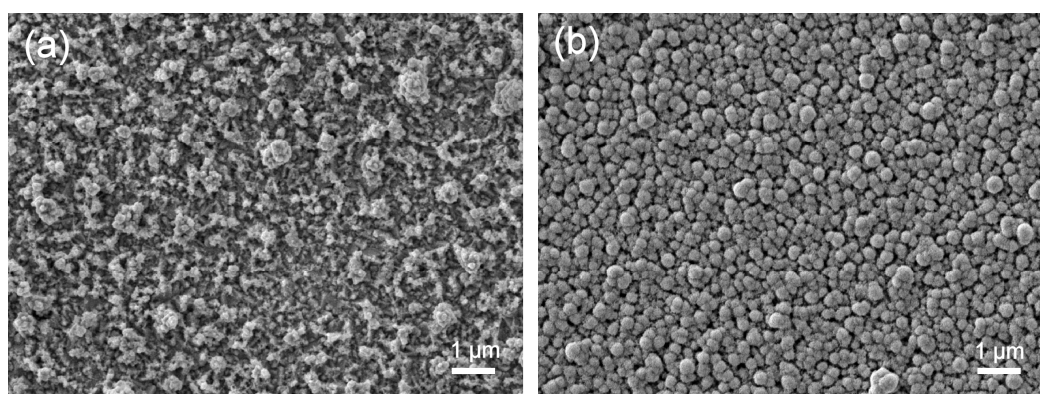

Figure 3. Top-view SEM images of electrodeposited $CuFeO_2$ films when applying a current density of -0.2 mA cm^{-2} for 60 min in DMSO based electrolytes with different potassium perchlorate concentrations: (**a**) Solution #1 containing 1 mM $Cu(NO_3)_2 \cdot xH_2O$/3 mM $Fe(ClO_4)_3 \cdot xH_2O$/100 mM potassium perchlorate and (**b**) Solution #2 containing 4 mM $Cu(NO_3)_2 \cdot xH_2O$/12 mM $Fe(ClO_4)_3 \cdot xH_2O$/50 mM potassium perchlorate. Electrodeposited films were annealed at 650 °C for 1 h under N_2 gas flow.

Deposition time is a main factor in controlling the thickness of an electrodeposited film. Figure 5 shows the cross-section SEM images of electrodeposited $CuFeO_2$ film with an applied current density of -0.1 mA cm^{-2} in the DMSO based electrolyte containing 1 mM $Cu(NO_3)_2 \cdot xH_2O$/3 mM $Fe(ClO_4)_3 \cdot xH_2O$/100 mM potassium perchlorate after post-annealing treatment at 650 °C under N_2 gas flow. The electrodeposition for 20 min produced a homogeneous nanostructured $CuFeO_2$ film with an average thickness of 500 nm, as shown in Figure 5a. The average thickness was increased to 875 nm after the electrodeposition for 40 min, as illustrated in Figure 5b. Finally, the nanostructured $CuFeO_2$ film with an average thickness of 1000 nm was electrodeposited for 60 min (Figure 5c). Interestingly, the surface of nanostructured $CuFeO_2$ film became rougher as the deposition time increased. In addition, the deposition of $CuFeO_2$ film became slow as the deposition time passed. In other words, it means that the deposition ratio over time was not linear. The rougher nanostructured $CuFeO_2$ film with the long deposition time was mainly due to the aggregation of $CuFeO_2$ particles, while the non-linear deposition ratio over time was likely to be due to the relatively low conductivity of the electrode by the pre-deposited $CuFeO_2$ film on the substrate.

In this way, it was demonstrated that electrodeposition in the DMSO based electrolyte containing more potassium perchlorate concentration with an applied current density of -0.1 mA cm^{-2} for deposition time below 30 min, and the post-annealing process at 650 °C under inert gas flow, produces nanostructured $CuFeO_2$ film with less aggregations. The XPS analysis also confirms the composition of this film in detail. Figure 6 shows the XPS spectra of the electrodeposited $CuFeO_2$ film in the DMSO based electrolyte containing 1 mM $Cu(NO_3)_2 \cdot xH_2O$/3 mM $Fe(ClO_4)_3 \cdot xH_2O$/100 mM potassium perchlorate with an applied current density of -0.1 mA cm^{-2} for 30 min after post-annealing treatment at 650 °C under N_2 gas flow: Cu 2p (Figure 6a), Fe 2p (Figure 6b), and O 1s (Figure 6c). In Figure 6a, peaks located at 932 eV and 952 eV correspond to the binding energies of Cu (I) $2p_{3/2}$ and Cu (I) $2p_{1/2}$, respectively. This confirms the monovalent state of Cu (Cu^+) in the $CuFeO_2$ film [46,47]. In Figure 6b, peaks located at 710 eV and 723 eV are derived from the

binding energies of Fe (III) $2p_{3/2}$ and Fe (III) $2p_{1/2}$, indicating the trivalent state of Fe (Fe^{3+}) in the $CuFeO_2$ film [46,47]. As shown in Figure 6c, the O 1s spectrum was deconvoluted into two peaks located at 529 eV and 530 eV, corresponding to the lattice oxygen species [48,49]. This is in good agreement with the typical chemical status of the crystalline $CuFeO_2$ in the literature [36]. Based on these compositional and morphological analyses, it was concluded that the DMSO based solution with more complexing agent concentrations is a suitable electrolyte for the electrodeposition bath to fabricate the nanostructured $CuFeO_2$ film without any impurities. In addition, it was demonstrated that it is possible to control the morphology of nanostructured $CuFeO_2$ film without any compositional transitions by changing the current density and deposition time of galvanostatic electrodeposition.
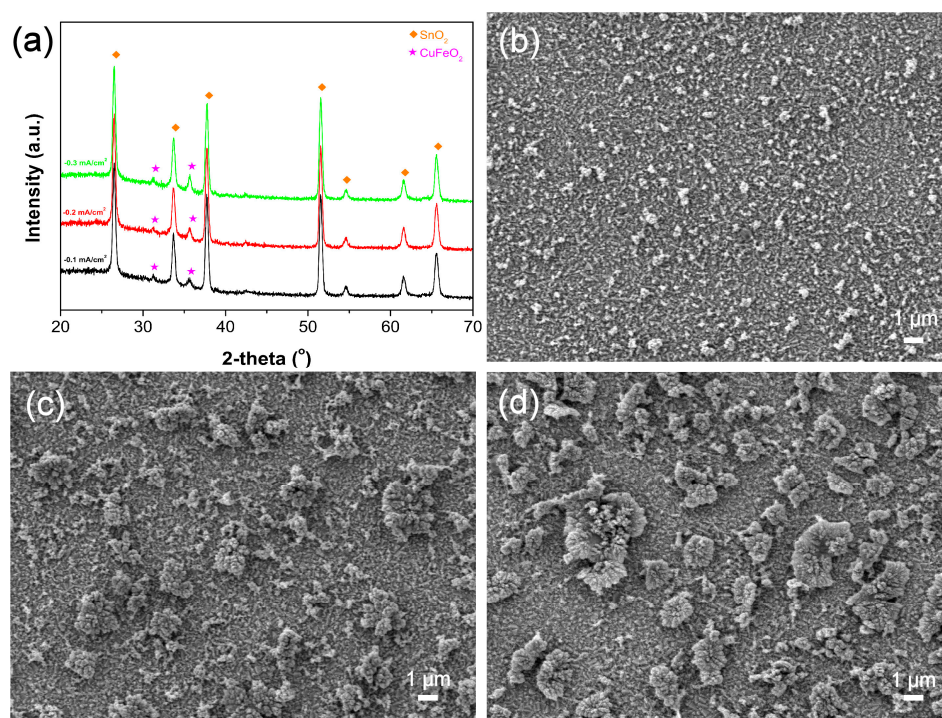

Figure 4. (**a**) XRD patterns of electrodeposited $CuFeO_2$ film by applying different current densities: -0.1 mA cm^{-2} (black), -0.2 mA cm^{-2} (red), and -0.3 mA cm^{-2} (green). Top view SEM images of electrodeposited $CuFeO_2$ film by applying different current densities of (**b**) -0.1 mA cm^{-2}, (**c**) -0.2 mA cm^{-2}, and (**d**) -0.3 mA cm^{-2}. Electrodeposition was carried out in DMSO based electrolytes containing 1 mM $Cu(NO_3)_2 \cdot xH_2O$/3 mM $Fe(ClO_4)_3 \cdot xH_2O$/100 mM potassium perchlorate for 30 min. Electrodeposited films were annealed at 650 °C for 1 h under N_2 gas flow.
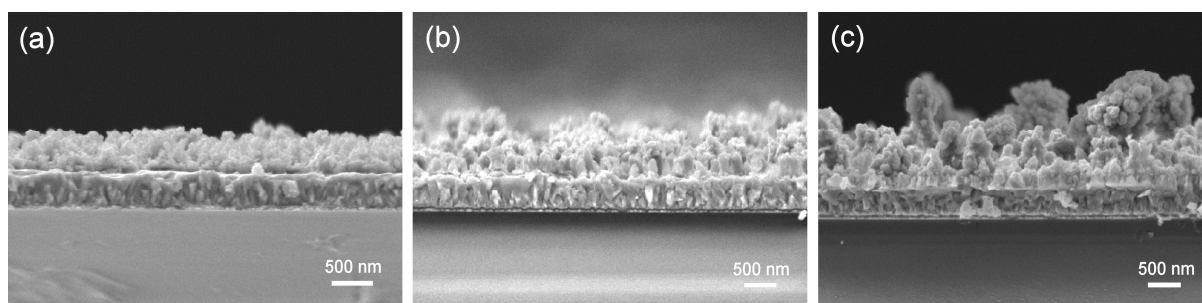

Figure 5. Cross-section SEM images of electrodeposited $CuFeO_2$ film with an applied current density of -0.1 mA cm^{-2} in DMSO based electrolyte containing 1 mM $Cu(NO_3)_2 \cdot xH_2O$/3 mM $Fe(ClO_4)_3 \cdot xH_2O$/100 mM potassium perchlorate for different deposition time: (**a**) 20 min (**b**) 40 min and (**c**) 60 min. Samples were annealed at 650 °C for 1 h under N_2 gas flow after electrodeposition.
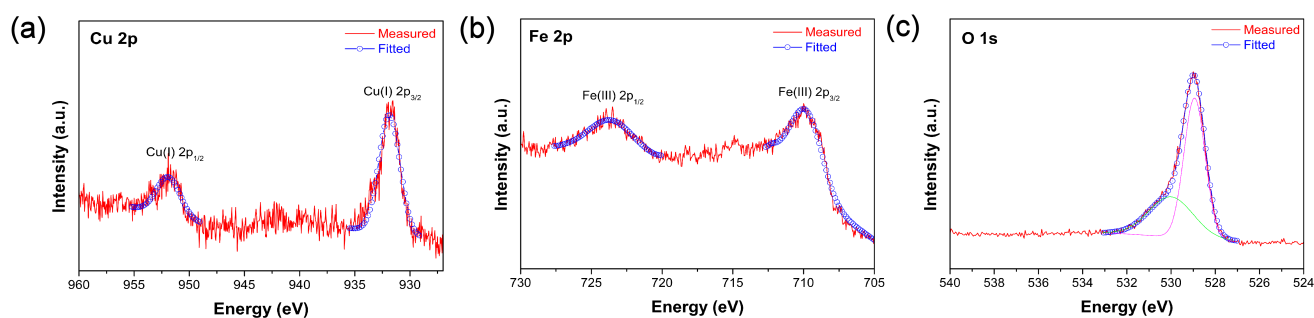
Figure 6. XPS spectra of electrodeposited $CuFeO_2$ film in DMSO based electrolyte containing 1 mM $Cu(NO_3)_2 \cdot xH_2O$/3 mM $Fe(ClO_4)_3 \cdot xH_2O$/100 mM potassium perchlorate with an applied current density of -0.1 mA cm^{-2} for 30 min after post-annealing treatment at 650 °C for 1hr under N_2 gas flow: (**a**) Cu 2p, (**b**) Fe 2p, and (**c**) O 1s.

4. Conclusions

In this study, the effect of deposition parameters, including the type of solvent, the condition of electrolyte, the applied current density and deposition time. on morphological and compositional characteristics of electrodeposited $CuFeO_2$ film was investigated. As a result, in terms of the solvent, nanostructured $CuFeO_2$ film was fabricated using the DMSO solution, while Cu_2O film was formed using the water solution. Furthermore, the concentration of potassium perchlorate as a complexing agent in the electrolyte caused morphological change in the electrodeposited $CuFeO_2$ film, as well as the compositional transition. On the other hand, the applied current density and deposition time did not have an influence on the composition of the electrodeposited $CuFeO_2$ film. However, they caused the morphological changes in the electrodeposited $CuFeO_2$ film. Along with previous studies (Table S1), it is expected that this will provide guidelines for selecting suitable electrodeposition conditions to fabricate nanostructured $CuFeO_2$ composite electrode for specific applications, such as solar energy conversion devices, temperature sensors, photocatalysts, magnetoelectric devices and transparent conductive substrates.

References

1. Chen, H.-Y.; Wu, J.-H. Transparent conductive $CuFeO_2$ thin films prepared by sol-gel processing. *Appl. Surf. Sci.* **2012**, *258*, 4844–4847. [CrossRef]

2. Deng, Z.; Fang, X.; Wang, X.; Wu, S.; Dong, W.; Shao, J.; Tao, R. Characterization of amorphous p-type transparent $CuFeO_2$ thin films prepared by radio frequency magnetron sputtering method at room temperature. *Thin Solid Film.* **2015**, *589*, 17–21. [CrossRef]

3. Mohamed, H.; Chikoidze, E.; Ratep, A.; Elsoud, A.M.A.; Boshta, M.; Osman, M.B.S. Synthesis of conducting single-phase $CuFeO_2$ thin films by spray pyrolysis technique. *Mater. Sci. Semicond. Process* **2020**, *107*, 104831. [CrossRef]

4. Elgazzar, E.; Tataroglu, A.; Al-Ghamdi, A.A.; Al-Tuki, Y.; Farooq, W.A.; El-Tantawy, F.; Yakuphanoglu, F. Thermal sensors based on delafossite film/p-silicon diode for low-temperature measurements. *Appl. Phys. A* **2016**, *122*, 617. [CrossRef]

5. Sinnarasa, I.; Thimont, Y.; Barnabe, A.; Beaudhuin, M.; Moll, A.; Schorne-Pinto, J.; Tailhades, P.; Presmanes, L. Microstructural and transport properties of Mg-doped $CuFeO_2$ thin films: A promising material for high accuracy miniaturized temperature sensors based on the Seebeck effect. *J. Alloys Compd.* **2020**, *827*, 154199. [CrossRef]

6. Xia, N.; Shi, L.; Xia, Z.; Chen, B.; Jin, Z.; Wang, Y.; Ouyang, Z.; Zuo, H.; Shen, Y. Dynamic behavior of magnetoelectric coupling of $CuFeO_2$ induced by a high magnetic field. *J. Appl. Phys.* **2014**, *115*, 114107. [CrossRef]

7. Dai, H.; Ye, F.; Li, T.; Chen, Z.; Cao, X.; Wang, B. Impact of Li doping on the microstructure, defects, and physical properties of $CuFeO_2$ multiferroic ceramics. *Ceram. Int.* **2019**, *45*, 24570–24577. [CrossRef]

8. Crespo, C.T. Potentiality of $CuFeO_2$-delafossite as a solar energy converter. *Sol. Energy* **2018**, *163*, 162–166. [CrossRef]

9. Read, C.G.; Park, Y.; Choi, K.-S. Electrochemical synthesis of p-type $CuFeO_2$ electrodes for use in a photoelectrochemical cell. *J. Phys. Chem. Lett.* **2012**, *3*, 1872–1876. [CrossRef]

10. Zhu, T.; Deng, Z.; Fang, X.; Huo, Z.; Wang, S.; Dong, W.; Shao, J.; Tao, R.; Song, C.; Wang, L. High photovoltages of $CuFeO_2$ based p-type dye-sensitized solar cells. *J. Alloys Compd.* **2016**, *685*, 836–840. [CrossRef]

11. Jin, Y.; Chumanov, G. Solution synthesis of pure 2H $CuFeO_2$ at low temperature. *RSC Adv.* **2016**, *6*, 26392–26397. [CrossRef]

12. Prevot, M.S.; Guijarro, N.; Sivula, K. Enhancing the performance of a robust sol-gel processed-type delafossite $CuFeO_2$ photocathode for solar water reduction. *ChemSusChem* **2015**, *8*, 1359–1367. [CrossRef]

13. Jang, Y.J.; Park, Y.B.; Kim, H.E.; Choi, Y.H.; Choi, S.H.; Lee, J.S. Oxygen-intercalated $CuFeO_2$ photocathode fabricated by hybrid microwave annealing for efficient solar hydrogen production. *Chem. Mater.* **2016**, *28*, 6054–6061. [CrossRef]

14. Oh, Y.; Yang, W.; Kim, J.; Jeong, S.; Moon, J. Enhanced photocurrent of transparent $CuFeO_2$ photocathodes by self-light-harvesting architecture. *ACS Appl. Mater. Interfaces* **2017**, *9*, 14078–14087. [CrossRef]

15. Boudoire, F.; Liu, Y.; Formal, F.L.; Guijarro, N.; Lhermitte, C.R.; Sivula, K. Spray synthesis of $CuFeO_2$ photocathodes and in-operando assessment of charge carrier recombination. *J. Phys. Chem. C* **2021**, *125*, 10883–10890. [CrossRef]

16. Prevot, M.S.; Jeanbourquin, X.A.; Bouree, W.S.; Abdi, F.; Friedrich, D.; Krol, R.; Guijarro, N.; Formal, F.L.; Sivula, K. Evaluating charge carrier transport and surface states in $CuFeO_2$ photocathodes. *Chem. Mater.* **2017**, *29*, 4952–4962. [CrossRef]

17. Liu, Q.-L.; Zhao, Z.-Y.; Zhao, R.-D.; Yi, J.-H. Fundamental properties of delafossite $CuFeO_2$ as photocatalyst for solar energy conversion. *J. Alloys Compd.* **2020**, *819*, 153032. [CrossRef]

18. Preethi, S.; Vivek, S.; Priya, R.; Balakumar, S.; Babu, K.S. Enhanced photocatalytic performance of $CuFeO_2$-ZnO heterostructures for methylene blue degradation under sunlight. *J. Mater. Sci. Mater. Electron.* **2021**, *32*, 22256–22269. [CrossRef]

19. Tu, L.-W.; Chang, K.-S. Hydrothermal fabrication and photocatalytic study of delafossite ($CuFeO_2$) thin films on fluorine-doped tin oxide substrate. *Mater. Chem. Phys.* **2021**, *267*, 124620. [CrossRef]

20. Barnabe, A.; Mugnier, E.; Presmanes, L.; Thailhades, P. Preparation of delafossite $CuFeO_2$ thin films by rf-sputtering on conventional glass substrate. *Mater. Lett.* **2006**, *60*, 3468–3470. [CrossRef]

21. Zhu, T.; Deng, Z.; Fang, X.; Dong, W.; Shao, J.; Tao, R.; Wang, S. Room temperature deposition of amorphous p-type $CuFeO_2$ and fabrication of $CuFeO_2$/n-Si heterojunction by RF sputtering method. *Bull. Mater. Sci.* **2016**, *39*, 883–887. [CrossRef]

22. Ziani, N.; Aubry, E.; Martin, N.; Hirsinger, L.; Billard, A.; Briois, P.; Belkaid, M.S.; Yazdi, M.A.P. Influence of substrate temperature on delafossite $CuFeO_2$ films synthesized by reactive magnetron sputtering. *J. Alloys Compd.* **2021**, *876*, 160169. [CrossRef]

23. Li, S.Z.; Liu, J.; Wang, X.Z.; Yan, B.W.; Li, H.; Liu, J.-M. Epitaxial growth of delafossite $CuFeO_2$ thin films by pulse laser deposition. *Phys. B Condens. Mater.* **2012**, *407*, 2412–2415. [CrossRef]

24. Joshi, T.; Senty, T.R.; Trappen, R.; Zhou, J.; Chen, S.; Ferrari, P.; Borisov, P.; Song, X.; Holcomb, M.B.; Bristow, A.D.; et al. Structural and magnetic properties of epitaxial delafossite $CuFeO_2$ thin films grown by pulsed laser deposition. *J. Appl. Phys.* **2015**, *117*, 013908. [CrossRef]

25. Luo, S.; Fluri, A.; Zhang, S.; Liu, X.; Döbeli, M.; Harrington, G.F.; Tu, R.; Pergolesi, D.; Ishihara, T.; Lippert, T. Thickness-dependent microstructural properties of heteroepitaxial (00.1) $CuFeO_2$ thin films on (00.1) sapphire by pulsed laser deposition. *J. Appl. Phys.* **2020**, *127*, 065301. [CrossRef]

26. Zhang, L.; Li, P.; Huang, K.; Tang, Z.; Liu, G.; Li, Y. Chemical solution deposition and transport properties of epitaxial $CuFeO_2$ thin films. *Mater. Lett.* **2011**, *65*, 3289–3291. [CrossRef]

27. Gupta, R.K.; Cavas, M.; Al-Ghamdi, A.A.; Gafer, Z.H.; El-Tantawy, F.; Yakuphanoglu, F. Electrical and photoresponse properties of Al/p-$CuFeO_2$/p-Si/Al MTCOS photodiode. *Sol. Energy* **2013**, *92*, 1–6. [CrossRef]

28. Ito, M.; Izawa, C.; Watanabe, T. Direct fabrication of a $CuFeO_2$/Fe photocathode for solar hydrogen production by hydrothermal method. *Chem. Lett.* **2017**, *46*, 814–816. [CrossRef]

29. Yuan, J.; Yang, L.; Hao, C. Lithium-doped CuFeO$_2$ thin film electrodes for photoelectrochemical reduction of carbon dioxide to methanol. *J. Electrochem. Soc.* **2019**, *166*, H718. [CrossRef]

30. Aqaei, F.; Zare, M.; Shafiekhani, A. Role of plasmonic Au nanoparticles embedded in the diamond-like carbon overlayer in the performance of CuFeO$_2$ solar photocathodes. *J. Solid State Electrochem.* **2021**, *25*, 1139–1150. [CrossRef]

31. Yin, G.; Liu, C.; Shi, T.; Ji, D.; Yao, Y.; Chen, Z. Porous BiVO$_4$ coupled with CuFeO$_2$ and NiFe layered double hydroxide as highly-efficient photoanode toward boosted photoelectrochemical water oxidation. *J. Photochem. Photobiol. A Chem.* **2022**, *426*, 113742. [CrossRef]

32. Alkhayatt, A.H.O.; Thahab, S.M.; Zgair, I.A. Structure, surface morphology and optical properties of post-annealed delafossite CuFeO$_2$ thin films. *Optik* **2016**, *127*, 3745–3749. [CrossRef]

33. Garcia-Torregrosa, I.; Geertzema, Y.G.; Ismail, A.S.M.; Lee, T.-L.; de Grioot, F.M.F.; Weckhyusen, B.M. Facile two-step synthesis of delafossite CuFeO$_2$ photocathodes by ultrasonic spray pyrolysis and hybrid microwave annealing. *ChemPhotoChem* **2019**, *3*, 1238–1245. [CrossRef]

34. Dharmadasa, I.M.; Haigh, J. Strengths and advantages of electrodeposition as a semiconductor growth technique for applications in microelectronic devices. *J. Electrochem. Soc.* **2006**, *153*, G47–G52. [CrossRef]

35. Xiao, F.; Hangarter, C.; Yoo, B.; Rheem, Y.; Lee, K.-H.; Myung, N.V. Recent progress in electrodeposition of thermoelectric thin films and nanostructures. *Electrochim. Acta* **2008**, *53*, 8103–8117. [CrossRef]

36. Riveros, G.; Garin, C.; Ramirez, D.; Dalchiele, E.A.; Marotti, R.E.; Pereyra, C.J.; Spera, E.; Gomez, H.; Grez, P.; Martin, F.; et al. Delafossite CuFeO$_2$ thin films electrochemically grown from a DMSO based solution. *Electrochim. Acta* **2015**, *164*, 297–306. [CrossRef]

37. Kang, U.; Park, H. A facile synthesis of CuFeO$_2$ and CuO composite photocatalyst films for the production of liquid formate from CO$_2$ and water over a month. *J. Mater. Chem. A* **2017**, *5*, 2123–2131. [CrossRef]

38. Yan, Z.; Liu, H.; Hao, Z.; Yu, M.; Chen, X.; Chen, J. Electrodeposition of (hydro)oxides for an oxygen evolution electrode. *Chem. Sci.* **2020**, *11*, 10614–10625. [CrossRef] [PubMed]

39. Oh, Y.; Yang, W.; Tan, J.; Lee, H.; Park, J.; Moon, J. Photoelectrodes based on 2D opals assembled from Cu-delafossite double-shelled microspheres for an enhanced photoelectrochemical response. *Nanoscale* **2018**, *10*, 3720–3729. [CrossRef]

40. Oh, Y.; Yang, W.; Tan, J.; Lee, H.; Park, J.; Moon, J. Boosting visible light harvesting in p-type ternary oxides for solar-to-hydrogen conversion using inverse opal structure. *Adv. Funct. Mater.* **2019**, *29*, 1900194. [CrossRef]

41. Wang, M.; Liu, C.; Shi, H.; Long, T.; Zhang, C.; Liu, B. Facile synthesis of chitosan-derived maillard reaction productions coated CuFeO$_2$ with abundant oxygen vacancies for higher Fenton-like catalytic performance. *Chemosphere* **2021**, *283*, 131191. [CrossRef]

42. Choudhary, S.; Sarma, J.V.N.; Pande, S.; Girad, S.A.; Turban, P.; Lepine, B.; Gangopadhyay, S. Oxidation mechanism of thin Cu films: A gateway towards the formation of single oxide phase. *AIP Adv.* **2018**, *8*, 055114. [CrossRef]

43. Luo, J.; Steier, L.; Son, M.-K.; Schreier, M.; Mayer, M.T.; Grätzel, M. Cu$_2$O nanowire photocathodes for efficient and durable solar water splitting. *Nano Lett.* **2016**, *16*, 1848–1857. [CrossRef] [PubMed]

44. Mamyrbekova, A.K.; Mamitova, A.D.; Turebekova, G.; Gul, K.; Mamyrbekova, A.K. Kinetics and mechanism of cathodic processes at electrolysis of Cu(NO$_3$)$_2$·3H$_2$O solution in dimethyl sulfoxide. *Asian J. Chem.* **2016**, *28*, 525–528. [CrossRef]

45. De, M.; Gupta, S.P.S. Lattice imperfection studies in polycrystalline materials by x-ray diffraction line-profile analysis. *Pramana* **1984**, *23*, 721–744. [CrossRef]

46. Chen, H.-Y.; Fu, J.-R. Delafossite-CuFeO$_2$ thin films prepared by atmospheric pressure plasma annealing. *Mater. Lett.* **2014**, *120*, 47–49. [CrossRef]

47. Xiong, D.; Qi, Y.; Li, X.; Tao, H.; Chen, W.; Zhao, X. Hydrothermal synthesis of delafossite CuFeO$_2$ crystals at 100 °C. *RSC Adv.* **2015**, *5*, 49280–49286. [CrossRef]

48. Li, Z.; Wu, W.; Wang, M.; Wang, Y.; Ma, X.; Luo, L.; Chen, Y.; Kan, K.; Pan, Y.; Li, H.; et al. Ambient-pressure hydrogenation of CO$_2$ into long-chain olefins. *Nat. Commun.* **2022**, *13*, 2396. [CrossRef] [PubMed]

49. Son, M.-K.; Seo, H.; Watanabe, M.; Shiratani, M.; Ishihara, T. Characteristics of crystalline sputtered LaFeO$_3$ thin films as photoelectrochemical water splitting photocathodes. *Nanoscale* **2020**, *12*, 9653–9660. [CrossRef] [PubMed]